ARCHIVES OF MECHANICS
Arch. Mech. **74** (2-3), 109–126, 2022, DOI: 10.24423/aom.3983

The stress-minimizing hole in a shear-loaded elastic plate at a given energy increment

S. VIGDERGAUZ

Research and Development Division, Israel Electric Corporation Ltd., P.O.Box 10, Haifa 31000, Israel, e-mail: ShmuelVigdergauz@Gmail.com

Minimization of the peak tangential stresses around a single hole in an infinite $2D$ elastic plate under remote pure shear and a given hole-induced strain energy level is considered as a free-shape optimization problem under a physical constraint. It is solved by combining a genetic algorithm with the almost analytical, and hence highly accurate stress-strain solver for any finitely parameterized family of closed curves. The results obtained in wide ranges of the governing parameters are detailed and discussed. They may be applicable to the optimal holes design in constructive elements and dilute perforated structures.
The current analysis extends the author's previous publications, which were focused on the unconstrained shape optimization within the same setup.

Key words: $2D$ elastostatic problem, Kolosov–Muskhelishvili potentials, stress concentration factor, shape optimization, effective energy, extremal elastic structures, genetic algorithm.

Copyright © 2022 by IPPT PAN, Warszawa

1. Background and motivation

Despite intensive studies carried out over the last decades, the problem of diminishing the weakening effect of construction holes in a flat elastic plate remains an object of much attention in engineering the optimal design. Various strengthening technologies, such as auxiliary unloading holes, reinforcement rings, and others, are known, each posing its own elastostatic problem. The proper shaping of holes, which may significantly improve the stress-strain state of perforated plates, is of particular assistance here. This optimization scheme is all the more promising as the hole area is usually much more important than its shape, which thus permits certain design freedom. For example, suppose the infinite plate has only a single traction-free hole and is loaded by remote pure shear. Though relatively simple, the considered setup is more challenging than the bulk-dominating load case, where the shape optimization problem is elliptic and permits a fully analytical 1-scale solution. This feature holds even for multiple interacting holes or foreign elastic inclusions at various geometries, including simply and doubly periodic structures (*the equistress shapes* – ESS, see [1] and references therein).

Quantitatively, the stress state of the plate is assessed by any of three interrelated criteria:

(A) the specific (per unit area of the hole) energy increment ΔW brought into a given outer stress field;

(B) the peak value K of the induced hoop stresses $\sigma_{\theta\theta}$ around the hole and;

(C) the stresses variation along the shape. Remarkably, no stress concentrations occur along the boundary in the ideal case of zero variation (a constant stress distribution). This relatively new assessment was advanced in [2]. The rigorous definition of the variation of a function on an interval is given in Section 2.

Interestingly and importantly for further analysis, the ESS provide the global minima for all three criteria simultaneously:

$$\min \Delta W \Longleftrightarrow \min K \Longleftrightarrow \sigma_{\theta\theta} = \text{const} \qquad \text{on the } ESS. \tag{1.1}$$

At shear loading, the ellipticity is no longer the case, and hence the ESS analogues simply do not exist. For this reason, the interrelations between the above criteria remain unsolved so far. Because of their analytical complexity, these can be studied only numerically.

Here, we address a non-trivial and challenging but also fascinating problem of numerically finding the optimal dependence between the local (B) and overall (A) quantities of the stress field

$$K(\Delta W) \to \min \tag{1.2}$$

around the stress-minimizing hole under remote shear. The hoop stresses variation (criterion C) remains outside the process and is analyzed *a posteriori* as a byproduct of the K minimization.

Any numerical optimization process includes an iteration scheme and a direct problem solver (DPS) repetitively used over various hole shapes. Both are of great importance for converging to the true optimum.

In this way, the main numerical difficulty is to provide the greatest possible accuracy of which the DPS is capable. Indeed, unlike two others, the stress peak value criterion (or stress concentration factor, SCF) is of *local* rather than *integral* nature and so is much more troublesome to achieve with high precision. To overcome this difficulty, we employ the almost analytical and very accurate K-solver proposed in [3] and subsequently used in solving other single hole elastostatic problems [4, 5].

Crucial here is that this DPS works equally well for any hole shape and remote load. Hence, it can be effectively embedded into a compact genetic algorithm (GA) engine for iterative searching of the K minimum at a given energy level ΔW with no prior gradient information required. Additionally, the GA is enhanced in efficiency and accuracy by the time-saving parametrization of a vast searching

space. For concreteness, we also assume that the hole possesses a p-fold rotational symmetry with $p \geq 4$.

The current study logically continues the author's previous paper [3] in which the global K minimization without presetting the energy threshold ΔW is numerically performed and analyzed for only $p = 4$ (a square-symmetric hole).

Our contribution here consists of:

(i) the numerical implementation of the above-sketched optimization tool to K minimization problem (1.2) in dependence on the energy level for representative intervals of the governing parameters ΔW and p;

(ii) obtaining a variety of numerical results, which turn out to be drastically different from those for the bi-axial case. They provide quantitative insight into the interrelation between the load-induced energy and stress peaks in free boundary optimization of 2D elastic structures, thus giving the exact lower bound on $K(\Delta W)$, which can be interpreted as the attainable dilute limit of the 1-scale perforated structures.

The remainder of this paper is organized as follows. For reader convenience, Section 2 summarizes the analytical basics required for further development. Section 3 sketches the fast and stable direct solver for evaluating the peak stress around an arbitrarily shaped hole. In terms of these tools, Section 4 formulates the exact shape optimization problem of numerically minimizing K under a lower constraint on a given energy level ΔW. The computational optimization scheme based on the genetic algorithm technique is briefly given in Section 5. Simulation settings and numerical results are presented and discussed in Section 6. Closing remarks are offered in Section 7.

2. Basic assumptions and governing equations

The setup in Fig. 1 is considered. Let an infinite thin plate be weakened by a hole with the p-fold rotationally symmetric boundary L_p enclosing the origin of coordinates in the plane E of a complex variable $z = x + iy \in E$. The curve L_p divides the plane in the hole region S_1 of a finite area f_1 and the unbounded region $S_2 = E \setminus S_1$ filled with an isotropic and linearly elastic phase. The plane is also remotely loaded by uniform non-tangential stresses

$$\sigma_{xx}^{\infty} = P, \quad \sigma_{yy}^{\infty} = Q, \quad \sigma_{xy}^{\infty} = 0, \tag{2.1}$$

while the hole's boundary is taken traction-free.

The load-induced stresses in the closed domain $S_2 + L_p$ are governed by the real-valued biharmonic Airy function. Though useful as a theoretical tool, it becomes ineffective in computing local stress and strain fields. Far more promising is the complex variable approach of equivalently replacing the Airy function

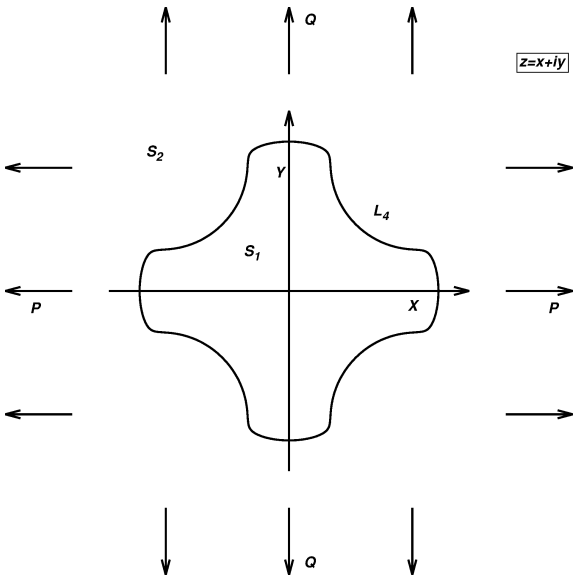

FIG. 1. An infinite plate with a traction-free hole under uniform stresses at infinity. The cases $P = Q$ and $P = -Q$ correspond to bulk and shear loading, respectively. The piecewise-smooth boundary of the hole has a p-fold rotational symmetry about the origin.

with a pair of complex-valued holomorphic functions $\Phi_0(z)$, $\Phi_0(z)$ (the Kolosov–Muskhelishvili potentials (KMP); see [6, 7]) interlinked along the material interface through given loading conditions. The resulting boundary value problem for them is then formulated and solved (analytically or numerically) using the complex variable machinery. To facilitate further derivations, we parameterize the shape L_p with a real angular variable θ along an auxiliary unit circle γ, also centered in the same origin:

$$L_p = \omega_p(\xi), \qquad \xi = \exp i\theta \in \gamma, \quad \overline{\xi} = \xi^{-1} \quad |\xi| = 1, \quad \theta \in [0, 2\pi], \tag{2.2}$$

where $\omega_p(\zeta)$ is the univalent ($\omega'(\zeta) \neq 0$) finite-term analytic function conformally mapping the exterior $\Sigma : |\zeta| \geq 1$ of γ onto the considered elastic domain $S + L_p$ with p-fold rotational symmetry:

$$\Sigma + \gamma \xrightarrow[\omega_p(\zeta)]{} S + L_p, \qquad \zeta = \rho \exp i\theta, \quad \rho \geq 1, \tag{2.3a}$$

$$\omega_p(e^{i\lambda_p}\zeta) = e^{i\lambda_p}\omega_p(\zeta) : \quad \omega_p(\zeta) = \zeta + \sum_{m=1}^{M} d_k \zeta^{1-mp}. \tag{2.3b}$$

Here $M \geq 1$ is an integer and $\lambda_p = 2\pi/p$ is the angular period of L_p. Without loss of generality, let L_p be placed symmetrically to the x-axis and, hence, the

coefficients $\{d_m\}$ are real. As design variables, they offer substantial numerical advantages detailed in [3]. For clarity, we display them here.

• They are "naturally" ordered, in the sense that the higher the coefficient, the lesser its impact on the inclusion shape. Indeed, from the geometrical point of view, the high-order mapping coefficients are mainly responsible for forming large curvature isolated shape points that are unlikely to appear in the SCF minimization process.

• They fall into the successfully narrowing intervals

$$-\frac{1}{\sqrt{mp-1}} \le d_m \le \frac{1}{\sqrt{mp-1}}, \qquad m = 1, 2, \dots, \tag{2.4}$$

following from non-negativity of the area f_1 inside γ [8]

$$f_1 = \pi\big(1 - (p-1)^2 d_1^2 - (2p-1)^2 d_2^2 - \dots\big) \ge 0. \tag{2.5}$$

This means that just a few first coefficients $\{d_k\}$ comprise by (2.4) a practically representative search pool Π_M of shapes – in contrast to, say, a necessarily dense representation through their nodal points.

• This on-circle parametrization is also useful technically since the following identities hold on γ, in contrast to any other shape

$$\overline{\xi} = \xi^{-1}, \qquad \int\limits_{\gamma} \overline{\xi}^m \xi^n d\xi = \int\limits_{\gamma} \xi^{n-m} d\xi = 2\pi i \delta_{m-n,1}, \qquad \xi \in \gamma, \tag{2.6}$$

where $\delta_{i,j}$ is the Kronecker delta, and a bar indicates complex conjugation. Moreover, the mutual orthogonality of (2.6) makes the stress-strain computations more manageable by applying the residues technique [8].

The transformed KMP in the auxiliary domain $\Sigma + \gamma$ are analytic functions with far-field asymptotics (2.1):

$$\Phi_0(\zeta) = B + \Phi(\zeta),\ \Psi_0(\zeta) = \Gamma + \Psi(\zeta);\quad \zeta \in \Sigma + \gamma,\quad \Phi(\zeta), \Psi(\zeta) = O(|\zeta|^{-2}), \tag{2.7a}$$

$$4B = Tr\{\sigma^{\infty}\} = Q + P,\ 2\Gamma = Dev\{\sigma^{\infty}\} = Q - P,\quad \operatorname{Im} B, \operatorname{Im} \Gamma = 0, \tag{2.7b}$$

and convergent series expansions

$$\Phi(\zeta) = \sum_{k=2}^{\infty} a_k \zeta^{-k}, \quad \Psi(\zeta) = \sum_{k=2}^{\infty} b_k \zeta^{-k}, \quad \zeta \in \Sigma + \gamma. \tag{2.8}$$

The first order items $\sim\zeta^{-1}$ in (2.8) must be zero to match the static state conditions [7].

Note that two basic cases of bulk ($B = 1$, $\Gamma = 0$) and shear ($B = 0$, $\Gamma = 1$) loadings correspond to isotopic and square antisymmetric (deviatoric) far stress field, respectively.

The hole-induced stresses are linearly related to $\Phi_0(\zeta), \Psi_0(\zeta)$ through the commonly-known formulae [7], which are not displayed here to save room.

Further, the zero tractions on $L_p : \sigma_{\rho\rho}(\xi) + i\sigma_{\rho\theta}(\xi) \equiv 0$ imply the following boundary condition on γ for the functions $\Phi(\zeta), \Psi(\zeta)$

$$-\frac{2}{\xi^2}\overline{\omega'(\xi)}[Re\Phi(\xi) + B] + \overline{\omega(\xi)}\Phi'(\xi) + \Gamma\omega'(\xi) = -\omega'(\xi)\Psi(\xi), \quad \xi \in \gamma. \tag{2.9}$$

The terms in (2.9) are rearranged specifically for later use.

We also note that far shear yields a zero average of the hoop stresses over γ

$$\overline{\sigma_{\theta\theta}} = \frac{1}{2\pi}\int_\gamma \sigma_{\theta\theta}(\theta)d\theta = 0. \tag{2.10}$$

At any given shape L_p, identities (2.7), (2.9) comprise together the direct boundary-value problem for $\Phi(\xi), \Psi(\xi)$. Specifically, the quantities of our interest are expressed through only the first potential $\Phi(\zeta)$ (see, for instance, [9])

$$\Delta W = \frac{4\pi a_2}{f_1}; \quad K = \max|\sigma_{\theta\theta}(\xi)| = 4\max|B + \mathrm{Re}\,\Phi(\xi)|, \quad 0 \le \xi \le \pi, \tag{2.11}$$

where a_2 is the second-order residue of $\Phi(\zeta)$ at $\zeta = 0$

$$\Phi(\zeta) = \frac{a_2}{\zeta^2} + o(|\zeta|^{-2}). \tag{2.12}$$

Further, by the theory of functions of a real variable the hoop stresses variation is defined through the non-negative sums [10], (see also [2])

$$V[\sigma_{\theta\theta}(L_p)] = \sup\sum_{i=0}^{n}|\sigma_{\theta\theta}(\theta_{i+1}) - \sigma_{\theta\theta}(\theta_i)| \ge 0, \quad \{\theta_i\} \in [0, \eta], \tag{2.13}$$

where the supremum is taken over all possible partitions of L_p with an arbitrary system of points $\theta_0, \theta_1 \ldots, \theta_n$ ordered by a chosen direction of traversing the irreducible half-period $\eta \le \pi$ of the angular stress distribution. For evident reason, we use only one such set in numerically evaluating the variations.

These are nontrivially bounded below [10] as

$$V[\sigma_{\theta\theta}] \ge \max(\sigma_{\theta\theta}(\theta)) - \min(\sigma_{\theta\theta}(\theta)), \quad \theta \in [0, \eta], \tag{2.14}$$

where the equal sign is true for only monotonic functions. Given this, we introduce the more suitable relative parameter

$$\rho = \frac{\max(\sigma_{\theta\theta}(\theta)) - \min(\sigma_{\theta\theta}(\theta))}{V[\sigma_{\theta\theta}]}, \quad 0 < \rho \le 1, \tag{2.15}$$

which is valid for any non-constant distribution $V[\sigma_{\theta\theta}] > 0$.

In particular, for a circular hole ($t \in L,\ |t|^2 = R^2,\ \omega(\xi) = \xi$) under unit shear, it is found analytically [7] that

$$\Phi(\xi) = \frac{R^2}{\xi^2}, \quad \Psi(\xi) = 3\frac{R^4}{\xi^4}, \qquad a_2 = R^2, \quad f_1 = \pi R^2, \quad \eta = \pi \tag{2.16}$$

and hence

$$\Delta W = 4, \quad \sigma_{\theta\theta}(\xi) = 4\cos 2\theta \implies K = 4, \quad V[\sigma_{\theta\theta}] = 4, \quad \rho = 1. \tag{2.17}$$

The relation $\rho = 1$ holds also for the antisymmetric stress distribution which changes the sign at the diagonal points $\theta = \pm\pi/4$ and $\theta = \pm 3\pi/4$ while keeping its modulus to hold (2.10) (the modular equistress principle)

$$|\sigma_{\theta\theta}(\xi)| = \text{const}, \qquad \xi \in \gamma. \tag{2.18}$$

Physically this corresponds to a step-wise distribution composed of four equal-length segments alternating between tensile and compressive uniform stresses of the same magnitude. Equation (2.18) is applied by [11] as a prerequisite for numerically identifying the energy-minimizing hole under remote shear at $p = 4$. The resultant suboptimal hole shapes look like a square with slightly rounded sides and pronounced corner angles close to the critical Carothers value $\approx 102.6^\circ$ [12], which provides no singularity at passing through the diagonals.

Expectedly, such a combination of flattening and local jumping in the trend of the stress distribution is also observed in the current $K(\Delta W)$ numerical minimization (Section 6) even though with unequal segments lengths and tensile/compressive stress levels.

3. One-potential direct solver

The KMP are uniquely solvable [7], at least for an arbitrary piecewise smooth hole shape which is the only factor influencing the problem's numerical severity. In actuality, however, there is a practical approach allowing to find $\Phi(\zeta)$ and $\Psi(\zeta)$ *almost analytically and in tandem rather than in parallel* for any finite-term mapping (2.3b).

Indeed, Eq. (2.9) states that its left side is the boundary value of a function holomorphic outside the unit circle γ and vanishing at infinity which thus has no non-negative powers of ζ as, in fact, taken in the Laurent series (2.8) for $\Psi(\xi)$. On the other hand, the substitution of the first expansion from (2.8) and (2.3b) into (2.9) does produce these powers with the coefficients composed of a_k, d_k and integers. The reason is the conjugation operation over $\zeta : \overline{\xi^k} = \xi^{-k}$,

$k = \pm 1, \pm 2, \ldots$. By necessarily equating them to zero, one gets an infinite system of linear algebraic equations [13] for $m = 0, 1, \ldots$

$$a_{m+2} - \sum_{k=1}^{m}(m-k+1)\overline{d}_{m-k+1}a_k - (m+1)\sum_{k=1}^{\infty}\overline{d}_{m+k+1}\overline{a}_k = A_m, \tag{3.1a}$$

$$A_0 = 2B - \Gamma,\ A_1 = 0,\ A_m = -2B(m+1)\overline{d}_{m+1}, \quad m \geq 2 \tag{3.1b}$$

in the unknowns $\{a_k\}$ only, with no coefficients of $\Psi(\xi)$. When needed, these can be restored afterward through (2.9) and (2.6).

The first sum in (3.1a) is omitted for $m = 0, 1$. In the case under study ($B = 0, \Gamma = 1$), the right-hand side of only the first equation ($m = 0$) is non-zero as well as the energy ΔW from (2.11) and hence the leading coefficient a_2. The latter implies that the half-period of the stress distribution $\eta = \pi$ for any odd and $\eta = \pi/2$ for any even $p \geq 4$. Higher coefficients and corresponding equations may partially vanish due to the interplay between the shear antisymmetry and adopted p-symmetry of the hole shape.

Remarkably, for any M-term finite mapping ($d_k = 0$, $\forall k > M$), the system (3.1) also shrinks to a finite number N of equations in the first non-zero unknowns a_k, $k = \overline{1, N}$ while the infinite remainder of them in the unknowns a_k, $k > N$ is next summed up *analytically* by a finite differences technique [3]. This possibility is a crucial point for further analysis. The finite system size N is defined by the lower of load and shape rotational symmetries. The bulk (isotropic) load always implies that $N = M$. At the same time, antisymmetric shear gives $N = M$ for $p = 4$ and $N = 2M$ for $p > 4$. For simplicity, we also assume here that p is even and equal at least to 4 to vanish all the odd coefficients $\{a_k\}$.

The net expression for the first potential $\Phi(\xi)$ reads [3]

$$\Phi(\xi) = \frac{R_N(\overline{\xi})}{\xi\omega'(\xi)}, \quad \xi \in \gamma, \tag{3.2}$$

where $R_N(\xi)$ is a polynomial of degree N in ξ

$$R_N(\xi) = r_N\xi^N + r_{N-1}\xi^{N-1} + \cdots + r_0, \tag{3.3}$$

with the coefficients

$$r_0 = a_1 = 0,\ \ r_1 = a_2,\ \ r_m = a_{m+1} - \sum_{k=2}^{m}(-1)^k k d_k a_{m+k+1}, \quad m \geq 2. \tag{3.4}$$

In other words, Eqs. (3.2)–(3.4) are *exact* up to negligible errors caused by numerically solving the well-defined system in the N first non-zero coefficients $\{a_k\}$ at moderate values of N.

Note that just this (almost) analytical solution of the direct problem within the GA process provides the numerical effectiveness of the SCF optimization in the finite M-dimensional search space Π_M of the design variables $\{d_1, d_2, \ldots, d_M\}$ all of them being bounded by the intervals (2.4).

4. Problem formulation

We aim to numerically minimize the stress concentration factor K over a wide search pool Π_M of shapes under a given degree of the shape's rotational symmetry p and energy decrement ΔW: $K = K(\Delta W)$ in a representative interval of their values. Especially significant is that these two enter the optimization search quite differently. While p is fixed at once for the whole search, ΔW is computed separately for each hole shape within $\{L_p\}$. Because of this, it is desirable to hold a chosen value ΔW^* with a one-sided inequality constraint,

$$\Delta W \geq \Delta W^*, \tag{4.1}$$

which forces GA to search for the SCF closest to the level $\Delta W = \Delta W^*$, provided the function $K(\Delta W)$ increases monotonically with ΔW.

This intuitively correct presumption is *a posteriori* justified by the numerical results obtained at discrete values of p for dense sets of values on representative intervals of ΔW as witnessed in Section 6.

With these preliminaries, we are now in a position to quantitatively rephrase the $2D$ shape optimization problem at hand in the above-defined terms:

Given a unit shear load at infinity and the rotational symmetry degree to find, over all admissible set of the design variables $\{d_m\}$, the p-symmetrical hole shape $L_p \in \Pi_M$ which minimizes the stress concentration factor K under constraint (4.1)*,*

$$K(L_p, M, \Delta W^*) \xrightarrow[\{d_m\}\in\Pi_M]{} \min(p, M, \Delta W^*). \tag{4.2}$$

This formulation is justified if and only if the criterion K converges rapidly to stable values with increasing M, and that is the case. In practice, our numerical simulations (Section 6) for $p = 4$ and $p = 6 \div 16$ become stable already at $M = 6 \div 8$ with the system size $N = 6 \div 8$ and $N = 12 \div 16$, respectively.

5. Computational optimization scheme

In general, there are two substantially different iterative strategies to choose from: gradient and non-gradient (stochastic) ones, each having its pros and cons, as detailed in [14] specifically for the structural optimization problems.

Here the shape optimization problem with a lower-bound constraint on the energy level ΔW is solved by minimizing the K criterion over an M-parameter set of closed curves. In principle, the single truncation approach (3.1)–(3.4) explicitly provides all the information required by standard gradient descent (directional) techniques. However, this results in too cumbersome analytical expressions and time-consuming calculations. A good alternative is a gradientless and hence more flexible genetic algorithm, which loosely mimics, both in the concept and in the terms, the natural selection principle of survival of the fittest borrowed from evolutionary biology.

Devised in the pioneering works [15] and [16], the GA finds wide application in engineering. Its current state of the art is given, for instance, in [17]. More specific information is detailed in the previous author's paper [3], where the basic GA is precisely adjusted and implemented in the closely related problem to identify the stress-minimizing hole under remote shear with no lower constraint (4.1) on the energy.

The search starts with an initial population of randomly generated binary strings (chromosomes), each encoding an individual shape through M mapping coefficients $\{d_k\}$. They are further subject to 1-point crossover, jump/creep mutations, and the elitist technique performed with pre-specified probabilities. The computed SCF of an individual is taken as its fitness so that the best individuals with the minimal fitness values have the highest chance of surviving through successive generations. Given this, wherever the constraint (4.1) is violated, the corresponding shape obtains a penalized fitness, and the GA process takes the next candidate. The idea is to make the shape non-competitive, assigning the penalty as the squared violation $(\Delta W^* - \Delta W)^2$ multiplied by a huge positive constant.

We use the same mechanism to weed out unfeasible self-intersecting shapes which may appear at each step since inequalities (2.4) are not sufficient to guarantee their absence. Unfortunately, no conditions in $\{d_k\}$ terms to detect self-intersections are known thus far. Therefore, we check each decoded curve for possibly breaking the monotonicity,

$$\frac{d \arg \omega(\theta)}{d\theta} \geq 0, \qquad \theta \in [0; \lambda_p], \tag{5.1}$$

which provides the more restrictive shape property of star-shapeness because, physically, only star-shaped holes are promising for K-minimization. All operations are performed with double-precision arithmetic (16 digits) to ensure a high-resolution search of the global optimum.

This process is governed by several control parameters that dictate its performance. Here, the parameters tuning is of lesser importance due to the relatively small problem size, as detailed at the end of the previous section. For this reason,

we use the parameters' values found in the unconstrained shape optimization [3]. They are not displayed here for brevity.

To ensure the accuracy of the results, they were computed several times, randomly starting each GA process and stopping it after a sufficiently large number of iterations when there is no more variation in the results.

6. Numerical simulations

To provide a reference point for the principal computations, we first find the global minimum of either of the two shape-dependent parameters K and ΔW with no lower bound (4.1) on its complement for different values of p (Table 1). The data for $p = 4$ are taken from [3]. The following points are noteworthy:

• The K- and ΔW-minimizing shapes differ from a circle with corresponding values of interest (2.17) only when $p = 4$ or 8 as computed here in the interval $p \in [4; 24]$. This result is partly given in [3] (and for $p = 6$ conjectured in [18]). The case $p = 8$ has not yet been analyzed in the literature.

• The only non-trivial starting cases $p = 4$ and (to a lesser extent) $p = 8$ are associated with markedly reduced K-criterion values than their energy minimum counterparts. The corresponding rows in Table 1 show that the gains are $(1 - 2.77936/3.243467) = 14.3\%$ and $(1 - 3.70496/4.0) = 7.3\%$, respectively, obtained at a slight sacrifice in the energy

$$\delta = \frac{\Delta W(K_{\min})}{\Delta W_{\min}} - 1 < 0.01\%. \tag{6.1}$$

This difference, even if very small, is detected owing to highly accurate computations with double precision arithmetic rather than resulted from round-off or discretization errors.

Table 1. The global (unconstrained) minima of K and ΔW, together with related quantities for different degrees p of rotational symmetry of the hole.

	K-optimization			ΔW-optimization		
p	$K_{\min}$	$\Delta W(K_{\min})$	$\rho(K_{\min})$	$K(\Delta W_{\min})$	$\Delta W_{\min}$	$\rho(\Delta W_{\min})$
4	2.77936	3.71770	0.97288	3.243467	3.71438	0.72777
6	4.0	4.0	1.0	4.0	4.0	1.0
8	3.70496	4.00187	0.98456	4.0	4.0	1.0
>8	4.0	4.0	1.0	4.0	4.0	1.0

The K-minimizing hole shapes and the resultant hoop stress distributions for $p = 4$ and 8 are shown in Fig 2. In contrast to the square-like hole at $p = 4$, the octagonally symmetric K-optimal shape is close to a circle (the dashed line in the upper inset of the figure) with slightly marked corners at $\theta_1 = 22.5^\circ$ and

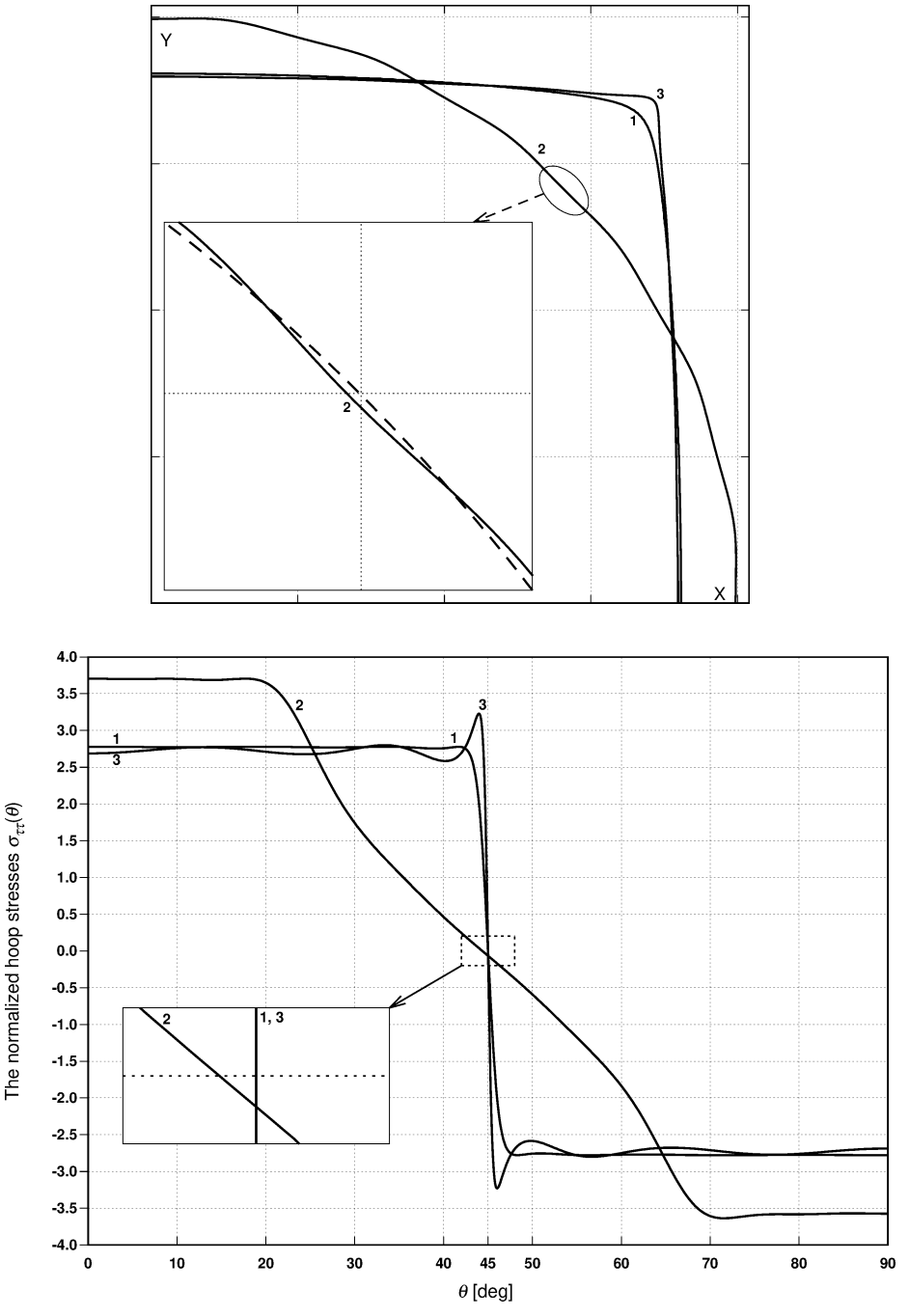

FIG. 2. The upper-right quarter of the unconstrained K-minimizing hole shapes (up) and the corresponding stress distributions (down) for $p = 4$ (1) and $p = 8$ (2). The energy-minimizing case for $p = 4$ (3) is also added for comparison.

$\theta_2 = 67.5°$. The corresponding optimal stress distribution consists of two strongly flattened parts, $\theta \in [0; \approx\theta_1]$, and $\theta \in [\approx\theta_2; 90°]$, with a gently curved line between them. Note that this is not an odd function about the point 45° as would be dictated by the modular equistress relations (2.18) for $p = 4$. Indeed, we have $\sigma_{\theta\theta}(0°) = 3.70496 \neq -\sigma_{\theta\theta}(90°) = 3.57359$ and $\sigma_{\theta\theta}(45°) = -0.06567 \neq 0$ (the bottom inset) – though the stresses average (2.10) is invariably zero as required by the shear load anti-symmetry for any p. For $p = 4$, we further contrast the discrepancy between K- and ΔW-optimal stress distributions. It is concentrated near a more pronounced angular point of the ΔW-optimal shape at $\theta = \pi/4$, where the local stress peak is formed to result in a modest lowering of the energy. On the other hand, the K stresses present a finite-term (and hence smoothed) approximation to a step function (2.18) with no peaks allowed.

The main result is summarized graphically in Fig. 3 where the dependence of K on the energy threshold is compared for different p. For easier comparison, we replace the absolute energy increment ΔW by the relative parameter $w = \Delta W/\Delta W_{\min}(p) : K_{\min}(\Delta W) \Rightarrow K_{\min}(w)$, where $\Delta W_{\min}(p)$ is the global energy minimum presented in the right-hand part of Table 1 so that $w \geq 1$ uniformly for any p. Since, because of (6.1), $K_{\min}(1+\delta) < K_{\min}(1)$ for $p = 4$ and 8, both curves first decline (as shown in an enlarged view at the bottom), and after fast reaching the nearby minimum, begin to rise with different slopes. The case $p = 4$ is seen to yield the smallest $K_{\min}$ at the same value of w, thanks to the mutual conformity of the load and hole rotational properties. This conclusion is quantitatively exemplified by comparing the K-minimization results at a particular threshold of $w = 1.05$. These are summarized in Table 2 and partially visualized in Fig. 4. For $p = 4$, the best K value is attended by a flattened (and hence more favorable) stress distribution with ρ very close to unity, unlike the oscillating distributions at $p = 6$ and 8 (Fig. 4, down) with much smaller ρ's. Note also that even at this relatively small energy constraint, the K-optimal shapes (Fig. 4, up) look markedly different from their counterparts under unconstrained optimization at $w = 1$ (Fig. 2, up). Whereas at $p = 6$ and 8,

Table 2. The constrained minima of K together with related quantities at the energy threshold $w = 1.05$ for different values of p

p	$K_{\min}$	$\Delta W(K_{\min})$	$\rho(K_{\min})$
4	3.27608	3.90010	0.99872
6	5.55670	4.2	0.46222
8	6.08143	4.2	0.33691
10	7.42158	4.2	0.33356
12	8.17853	4.2	0.24977
16	9.16804	4.2	0.16708

the shapes tend to form p-periodic bulges, the square symmetric hole boundary becomes close to a circle. Its further evolution versus the increasing values of w is displayed in Fig. 5 together with the corresponding stress distributions.

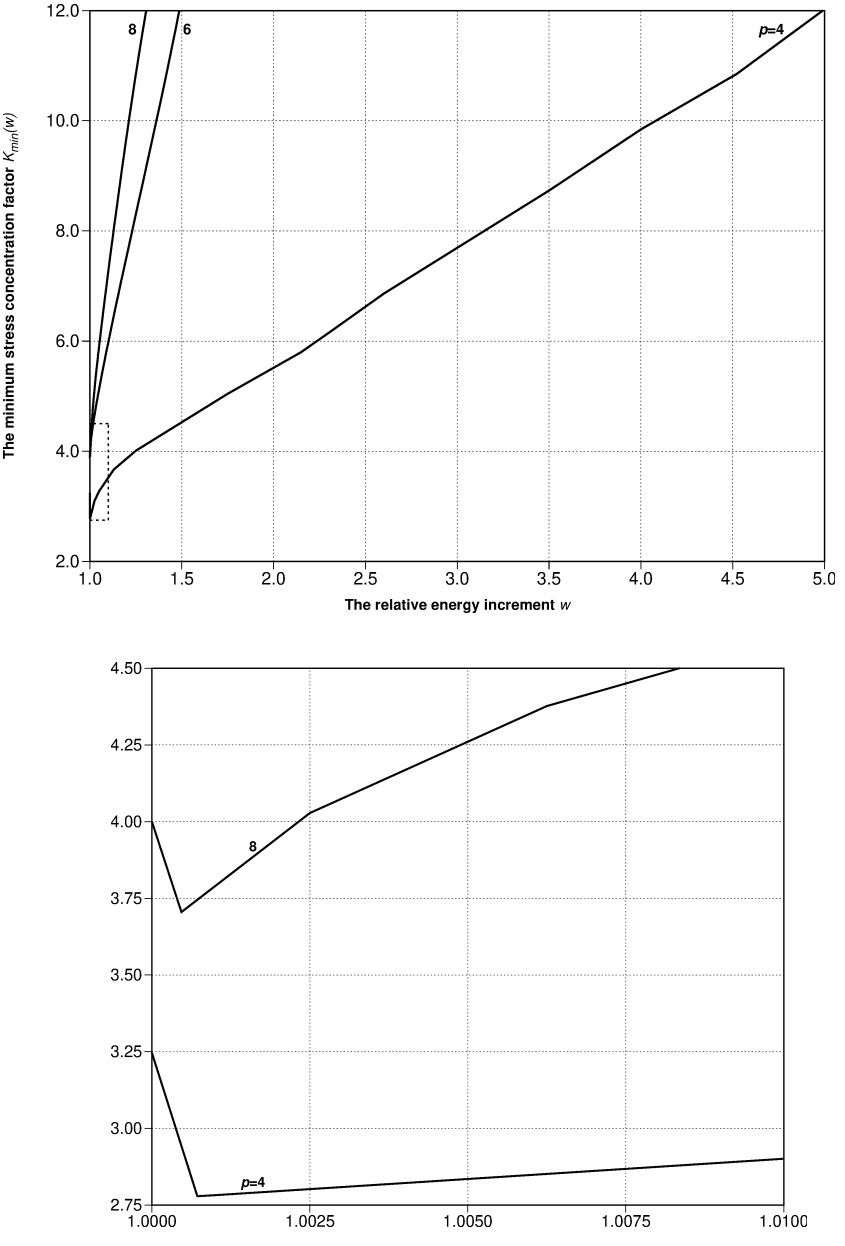

FIG. 3. The min $K_{\min}(w)$ dependence for different degrees p of the hole's rotational symmetry. An enlarged view of the dotted square near $w = 1$ is given in the below figure.

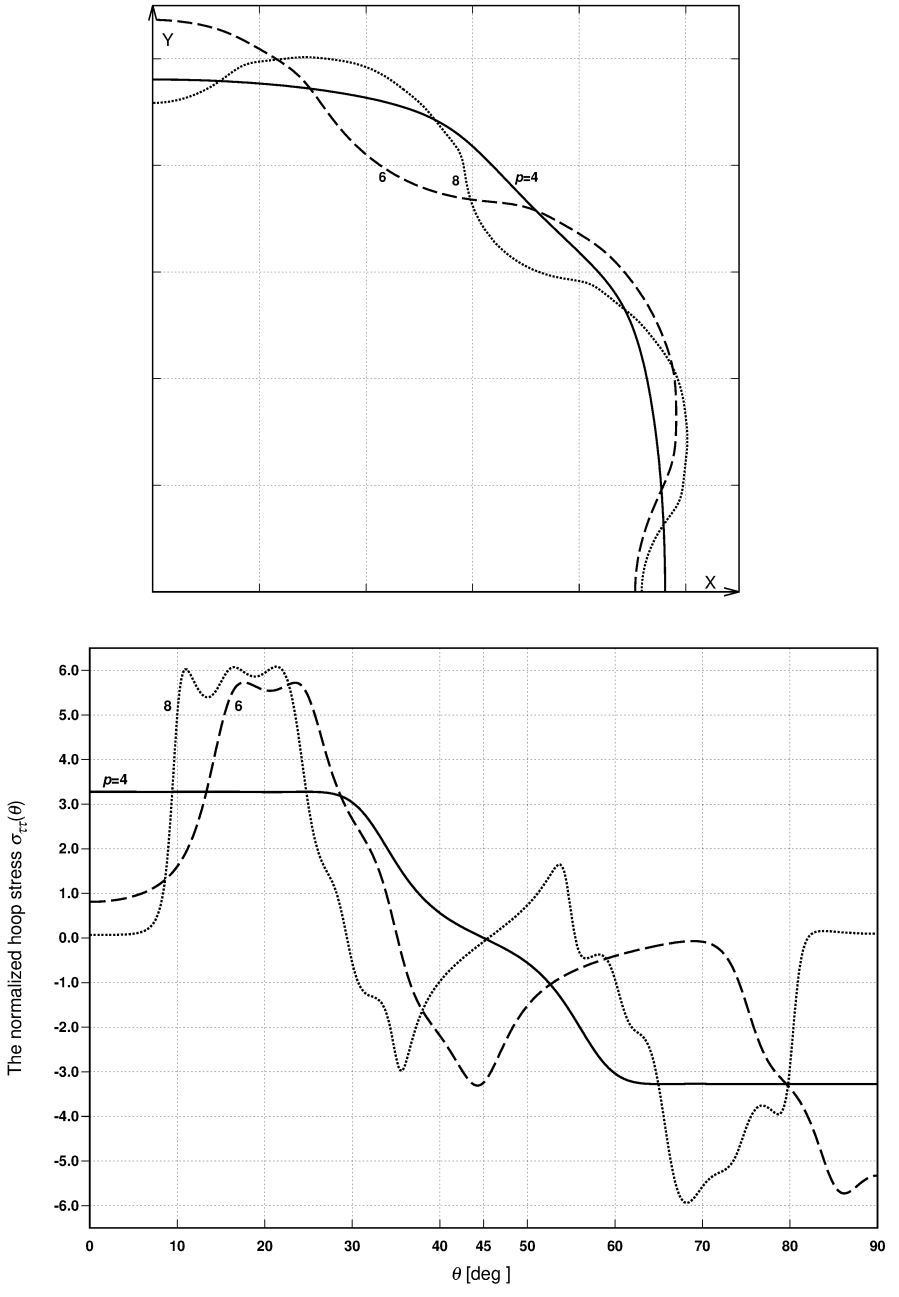

FIG. 4. The upper-right quarter of the bounded K-minimizing hole shapes (up) and the corresponding stress distributions (down) at the energy threshold $w = 1.05$ for $p = 4, 6, 8$ (the solid, dashed, and dotted line, respectively).

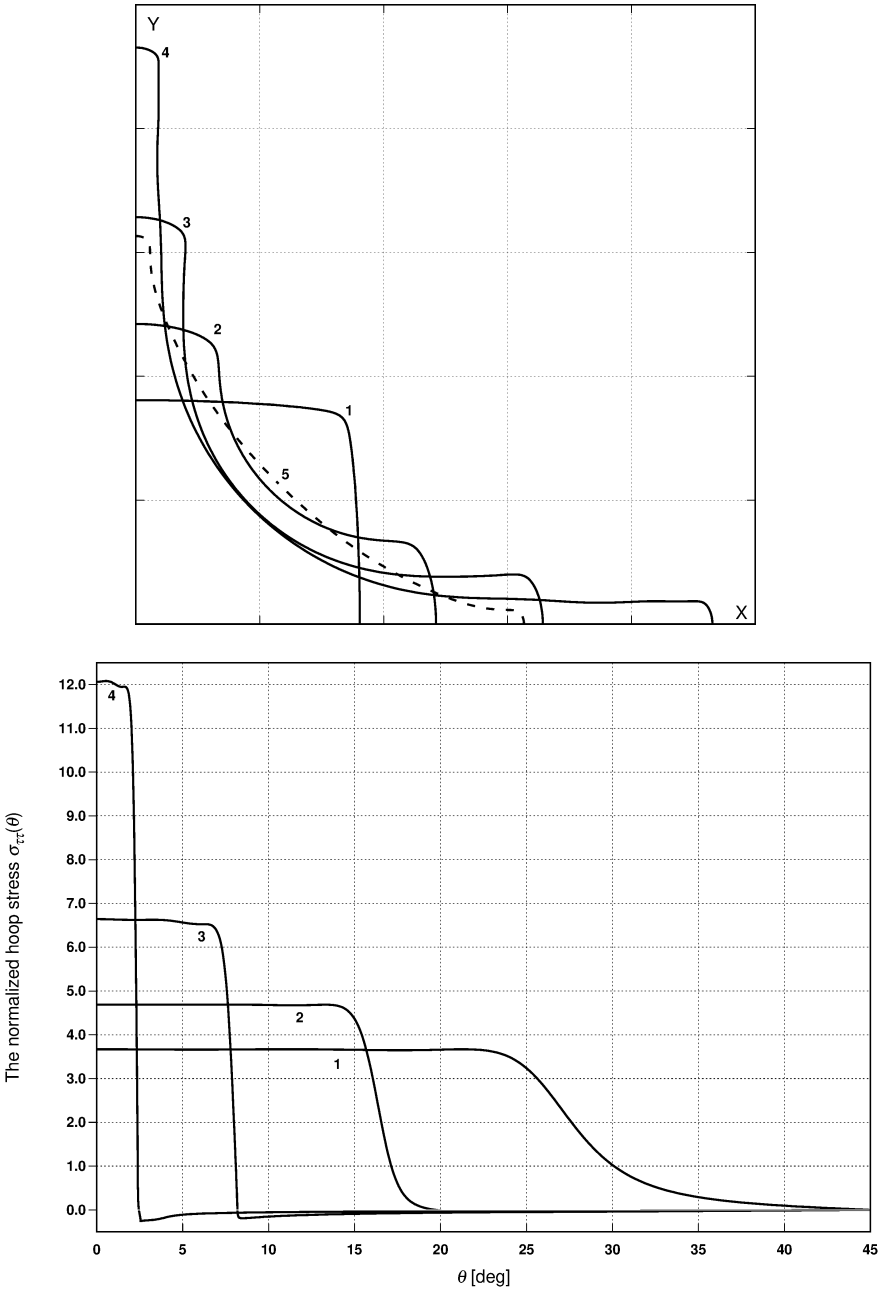

FIG. 5. The upper-right quarter of the bounded K-minimizing hole shapes (up) and the corresponding stress distributions (down) for $p = 4$ and increasing values of $w > 1$: 1 – ($w = 1.13$, $K_{min} = 3.669$, $\rho = 0.984$), 2 – (1.50, 4.688, 0.984), 3 – (2.60, 6.643, 0.972), 4 – (5.0, 12.079, 0.978).

The attention is drawn to the resultant smoothly-shaped "arms" along the load axes, gradually lengthening to match the growing constraint w. Expectedly, the K-optimal stress distributions tend to be almost piecewise constant, smoothly truncated across the arm's vertices, with the relative variation ρ remaining close to unity in a wide interval of the energy values. Thus, we conclude cautiously that the step-like distribution pattern and $\min K$ are positively correlated at the same w. It makes the results obtained more meaningful for engineering practice.

7. Conclusions

The paper presented a GA-based study of a rather challenging $2D$ shape optimization problem of minimizing the stresses around a hole in a shear-loaded plane with a one-sided constraint on the induced energy. This was achieved in a complex-variable framework by combining the highly accurate direct problem solver with the flexible and efficient shape parametrization. For clarity, we repeat here the essential points of the approach.

First, the parameterizing function (2.3b) is taken to contain only a small finite number M of terms used as the design variables. This assumption is physically motivated and numerically justified because their optimal values invariably fall well inside the allowed intervals (2.4).

Further, the fitness of each candidate from the searching space is calculated by the high-precision finite algorithm with no numerical integration or other approximative operations.

Finally, the conditional $K(w)$-minimization problem is solved numerically for different values of p by the easy to adapt and to use GA searching engine, which straightforwardly incorporates the energy constraint.

The results so obtained provide detailed information regarding to the interaction between the SCF and energy levels far beyond the global minimum case considered in [11], [19], and [3].

Nevertheless, it has to be stressed the direct solver used here works only for a single hole and may not be extended to several interacting ones where other approaches [20, 21] are successfully used instead.

References

1. S. VIGDERGAUZ, *Shape optimization in an elastic plate under remote shear: from single to intercting holes*, Journal of Mechanics of Materials and Structures, **3**, 7, 1341–1363, 2008.
2. S. VIGDERGAUZ, *A generalization of the equi-stress principle in optimizing the mechanical performance of two-dimensional grained composites*, Mathematics and Mechanics of Solids, **18**, 4, 431–445, 2013.

3. S. VIGDERGAUZ, *Stress-minimizing hole in an elastic plate under remote shear*, Journal of Mechanics of Materials and Structures, **1**, 2, 387–406, 2006.

4. S. VIGDERGAUZ, I. ELISHAKOFF, *Energy-minimizing holes in an elastic plate under remote loading*, Journal of Mechanics of Materials and Structures, **14**, 1, 139–154, 2019.

5. S. VIGDERGAUZ, I. ELISHAKOFF, *Stress-minimizing holes with a given surface roughness in a remotely loaded elastic plane*, Journal of Mechanics of Materials and Structures, **15**, 1, 1–14, 2020.

6. A.H. ENGLAND, *Variable Methods in Elasticity*, Springer, Berlin, 2009.

7. N.I. MUSKHELISHVILI, *Some basic Problems of the Mathematical Theory of Elasticity*, 2nd ed., Noordhoff, Leiden, the Netherlands, 1975.

8. T.W. GAMELIN, Complex Analysis, Springer, UTM, 2003.

9. I. JASIUK, *Cavities vis-a-vis rigid inclusions: elastic moduli of materials with polygonal inclusions*, International Journal of Solids and Structures, **32**, 3/4, 407–422, 1995.

10. N.L. CAROTHERS, *Real Analysis*, Cambridge University Press, International ed., 2009.

11. S. VIGDERGAUZ, A. CHERKAEV, *A hole in a plate optimal for its biaxial extension-compression*, Journal of Applied Mathematics and Mechanics, **50**, 3, 401–404, 1986.

12. S.D. CAROTHERS, *Plane strain in a wedge*, Proceedings of the Royal Society of Edinburgh, **23**, 292, 1912.

13. A.I. KALANDIA, *Mathematical Methods of Two-dimensional Elasticity*, Mir, Moscow, 1975.

14. O. SIGMUND, *On the usefulness of non-gradient approaches in topology optimization*, Structural and Multidisciplinary Optimization, **43**, 5, 589–596, 2011.

15. I. RECHENBERG, *Evolutionsstrategie – Optimierung technischer Systeme nach Prinzipien der biologischen Evolution*, Friedrich Frommann Verlag, Stuttgard, 1973.

16. J.H. HOLLAND, *Adaptation in Natural and Artificial Systems*, University of Michigan Press, Ann-Arbor, Michigan, 1975.

17. O. KRAMER, *Genetic Algorithm Essentials*, Springer International Publishing, Switzerland, 2017.

18. S. TORQUATO, L.V. GIBIANSKY, M.J. SILVA, L.J. GIBSON, *Effective mechanical and transport properties of cellular solids*, International Journal of Mechanical Sciences, **40**, 1, 71–82, 1998.

19. A.V. CHERKAEV, Y. GRABOVSKY, A.B. MOVCHAN, S.K. SERKOV, *The cavity of optimal shape under shear stresses*, International Journal of Solids and Structures, **35**, 33, 4391–4410, 1998.

20. G. ALLAIRE, F. JOUVE, H. MAILLOT, *Topology optimization for minimum stress design with the homogenization method*, Structural and Multidisciplinary Optimization, **28**, 87–98, 2004.

21. A. FERRER, P. GEOFFROY-DONDERS, G. ALLAIRE, *Stress minimization for lattice structures, part I: Micro-structure design*, Transactions of the Royal Society A, **379**, 2021.

Received January 15, 2022; revised version April 6, 2022.
Published online April 24, 2022.